Since January 2020 Elsevier has created a COVID-19 resource centre with free information in English and Mandarin on the novel coronavirus COVID-19. The COVID-19 resource centre is hosted on Elsevier Connect, the company's public news and information website.

Colloids and Surfaces B: Biointerfaces 203 (2021) 111724

Contents lists available at ScienceDirect

Colloids and Surfaces B: Biointerfaces

journal homepage: www.elsevier.com/locate/colsurfb

Antiviral zinc oxide nanoparticles mediated by hesperidin and *in silico* comparison study between antiviral phenolics as anti-SARS-CoV-2

Gouda H. Attia [a,b], Yasmine S. Moemen [c], Mahmoud Youns [d], Ammar M. Ibrahim [e], Randa Abdou [f,g], Mohamed A. El Raey [h,*]

[a] Department of Pharmacognosy, College of Pharmacy, Najran University, Najran, Saudi Arabia
[b] Department of Pharmacognosy, Faculty of Pharmacy, Kafr El-Shiekh University, Kafr El-Shiekh, Egypt
[c] Clinical Pathology Department, National Liver Institute, Menoufia University, Menoufia, Egypt
[d] Department of Biochemistry and Molecular Biology, Faculty of Pharmacy, Helwan University, Cairo, Egypt
[e] Applied Medical Sciences College, Najran University, Najran, Saudi Arabia
[f] Department of Pharmacognosy, Faculty of Pharmacy, Umm Al-Qura University, Makkah, Saudi Arabia
[g] Department of Pharmacognosy, Faculty of Pharmacy, Helwan University, Cairo, Egypt
[h] Department of Phytochemistry and Plant Systematics, Pharmaceutical Division, National Research Centre, Dokki, Cairo, Egypt

ARTICLE INFO

Keywords:
SARS-CoV-2
Nutraceuticals
Molecular docking
Zinc oxide nanoparticles
Hesperidin

ABSTRACT

Severe acute respiratory syndrome coronavirus 2 (SARS-CoV-2), which caused the coronavirus (COVID-19), is the virus responsible for over 69,613,607 million infections and over 1,582,966 deaths worldwide. All treatment measures and protocols were considered to be supportive only and not curative. During this current coronavirus pandemic, searching for pharmaceutical or traditional complementary and integrative medicine to assist with prevention, treatment, and recovery has been advantageous. These phytopharmaceuticals and nutraceuticals can be more economic, available, safe and lower side effects. This is *in silico* comparison study of ten phenolic antiviral agents against SARS-CoV-2, as well as isolation of the most active metabolite from natural sources. Zinc oxide nanoparticles (ZnO NPs) were also then prepared using these metabolite as a reducing agent. All tested compounds showed predicted anti-SARS-CoV-2 activity. Hesperidin showed the highest docking score, this leads us to isolate it from the orange peels and we confirmed its structure by conventenional spectroscopic analysis. In addition, synthesis of hesperidin zinc oxide nanoparticles was characterized by UV, IR, XRD and TEM. *In vitro* antiviral activity of hesperidin and ZnO NPs was evaluated against hepatitis A virus as an example of RNA viruses. However, ZnO NPs and hesperidin showed antiviral activity against HAV but ZnO NPs showed higher activity than hesperidin. Thus, hesperidin and its mediated ZnO nanoparticles are willing antiviral agents and further studies against SARS-CoV-2 are required to be used as a potential treatment.

1. Introduction

The current COVID-19 pandmic is responsible for over 69 million infections and over 1.5 million deaths worldwide to date, 2.3 million infections and more than 55,000 deaths in Africa, and over 119,000 infections and more than 6000 deaths in Egypt [1]. In most individuals infected with SARS-CoV-2 symptoms include mild to moderate respiratory disease that might recover without physician consultation. However, individuals with chronic diseases such as cardiovascular disease, diabetes, chronic respiratory disease or cancer have a greater risk of developing acute respiratory symptoms. COVID-19 transmission is prevented by maintaining social distance, washing hands or using alcohol sterilization, and not touching the face. Where it transmit through droplets of saliva from the person nose when an infected individual coughs or sneezes [1]. All measures and protocols were considered to be only supportive but not curative. However, there are many current clinical trials evaluating potential drugs [1]. Since claiming COVID-19 as a global pandemic there was a necessity to search for pharmaceutical or traditional, complementary and integrative medicine to assist with prevention, treatment and recovery [2].

Natural products are untapped sources for compounds that can be used in the prevention and treatment of different diseases. In addition,

* Corresponding author at: Phytochemistry &Plant Systematics Department, Pharmaceutical Research Division, National Research Centre, 33 El Bohouth St. Dokki, P.O. Box 12622, Cairo, Egypt.
E-mail address: ma.aziz@nrc.sci.eg (M.A. El Raey).

https://doi.org/10.1016/j.colsurfb.2021.111724
Received 3 January 2021; Received in revised form 16 March 2021; Accepted 24 March 2021
Available online 26 March 2021

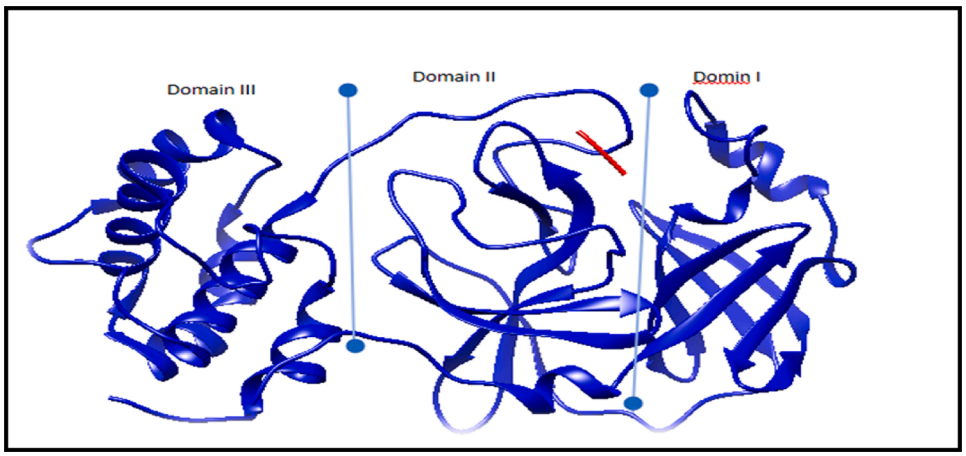

Fig. 1. Main protease (6lu7) was been classified according to their domain regions; domain I (residues 8–101), domain II (residues 102–184) with an antiparallel β-sheet structure and domain III (residues 201–303) which was been arranged in an α helix, as well as cleft region between domain II and III (residues 185–200) [8].

natural compounds have often served as cheaper and safer drug candidates against several diseases, many nutraceutical compounds were reported to have antiviral activities [3].

In the last decade, the number of new antiviral drugs extracted from natural sources has risen significantly. Natural products assist in the discovery of antiviral medicines, either directly or indirectly [4].

Therefore, screening of natural compound libraries by computational screening methods as molecular docking can save both time and money in drug development [3]

On the other hand, Znic (Zn)-containing compounds have shown antiviral properties toward a number of viruses according to such physical processes such as attachment of virus, virus infection, and uncoating. In addition to the inhibition of viral protease and polymerase [5]. Generally, Zn is an essential element that found in tissues of our bodies such as the muscle, brain, skin, bone. It is also an essential component of different enzyme system involved in metabolism and nucleic acid and protein biosynthesis [5].

It should be noted that, ZnO NPs are more easily absorbed by the body than zinc itself. ZnO NPs are currently utilized in the food industry as additive and in packaging. Furthermore, ZnO was categorized as safe substance by the US Food and Drug Administration. Therefore, ZnO NPs are attractive for use in biomedical applications. ZnO NPs are characterized by their low economic cost and low toxicity, therefore, ZnO NPs can be widely used for biomedical applications as antibacterial, anticancer, antidiabetic, anti-inflammatory, drug delivery and wound healing [6].

Zn-containing compounds were recently reported to display anti-SARS-CoV-2 activity [7] Thus, Zn-containing drugs are commonly prescribed in COVID-19 protection protocols. Consequently, green synthesis of ZnO NPs merits specific attention.

In this work, a number of phytopharmaceutical phenolic compounds from commonly used medicinal plants and foods (nutraceuticals) undergo *in silico* molecular study to explore antiviral activity against SARS-CoV-2 main protease (M^{pro}) and experimentally the highest docking score compound will be tested beside its mediated ZnO nanoparticles against the Hepatitis A virus (HAV), an RNA virus similar to SARS−COV-2.

2. Materials and methods

2.1. Molecular docking

The main protease (M^{pro}) is an important enzyme encoded by the coronavirus genome, with an essential role in virus replication and transcription process, making it a suitable drug target for SARS-CoV-2. To reveal the inhibition mechanism of selected polyphenolic compounds such as rutin, coirlagin, diosmin, myricetin-3-*O*-xylosyl-(1→2)-rhamnoside, epigallocatechin-3-*O*-gallate, hesperidin, lyoniresinol, myricetin, naringenin and quercetin 3-*O*-glucouronide versus the crystal structure of SARS-CoV-2 M^{pro} (6lu7) [8] which were used with a resolution of 2.1 A°. It was used for *in silico* molecular docking. This protein is composed of two polypeptides known as protomers A and B. This dimer has a crystallographic symmetry along two fold axis. It contains three domains; domain I (residues 8–101), domain II (residues 102–184) with an antiparallel β- sheet structure and domain III (residues 201–303) has five α-helices arranged as antiparallel spherical cluster. Where domain III connected to domain II by a long loop region (residues 185–200). SARS-CoV-2, M^{pro}, has a Cys-His coupled catalytic activity, where the substrate-binding site is located in a cleft between domain I and domain II [8] as in Fig. 1. In the current study, molecular docking procedures were executed by the Swiss Dock service [9]. Using EADock DSS, which perform blind docking and its CHARMM energies were assessed on a grid where the most favorable energies were estimated with FACTS and clustered. These clusters can be visualized and interpreted using Chimera as reported in literature [10].

2.2. Plant materials, extraction and isolation

Orange peels (500 g) were purchased from a local juice factory. Orange peels (200 g) were extracted with 2 L of hot distilled water till exhaustion. The extract was filtered and evaporated to become more concentrated under vacuum. The water extract was partitioned by CH_2Cl_2 followed by butanol. The butanol subfraction was applied to Whatman filter paper sheets 3 MM using BAW as eluent [12,11] to yield a major dark purple band under ultraviolet (UV) light. The dark purple band was isolated and macerated in methanol, then evaporated under vacuum using rotatory evaporator. The dried material applied to a Sephadex LH -20 column using EtOH/H_2O (1:1) as eluent to yield 120 mg of hesperidin.

2.3. Nuclear magnetic resonance (NMR)

^{1}H-nuclear magnetic resonance (NMR) spectra were recorded on a Bruker avance III, 400 MHz NMR spectrometer and 100 MHz for ^{13}C-NMR. ^{1}H chemical shifts (δ) were measured in ppm, relative to TMS and ^{13}C-NMR chemical shifts to dimethyl sulfoxide-d_6 and converted to the TMS scale by adding 39.5.

2.4. Synthesis of zinc oxide nanoparticles (ZnO NPs)

ZnO NPs were synthesized using by a method described by Attia et al. [13], in which 50 mg of hesperidin dissolved in 5 mL of DMSO mixed

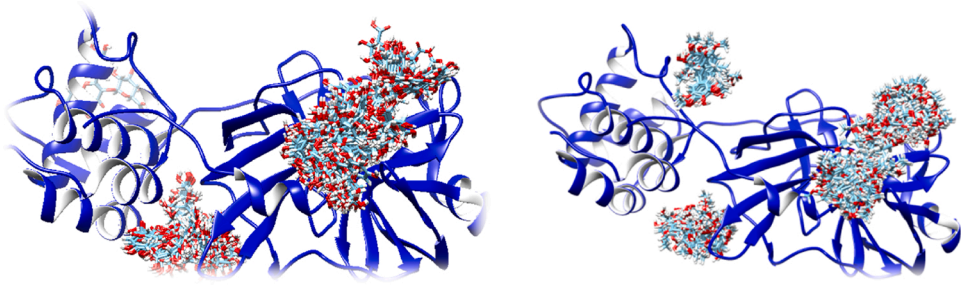

Fig. 2. Hesperidin (left) and lyoniresinol (right) with all possible conformations docked to the main protease (6lu7).

with 500 mg of zinc acetate dissolved in 50 mL bi-distilled water and heated in boiling water bath for 20 min. Five drops of ammonium hydroxide was then added to the reaction to raise the pH to 12, where a ZnO NPs precipitate is formed. The mixture was left for half an hour for complete reduction of zinc acetate to ZnO NPs. The formed precipitate was centrifuged at 8000 rpm, followed by washing two times by bi-distilled water, and two washes with ethanol to yield white pellets of ZnO NPs upon freeze drying.

2.5. Characterization of metal nanoparticles

2.5.1. UV–vis spectral analysis

ZnO NPs preparations were examined using a UV spectrophotometer, Shimadzu, UV-1601 (Shimadzu Corporation, Japan). The UV spectra recorded between 200−400 nm.

2.5.2. FT-IR analysis

The functional groups of the synthesized zinc oxide nanoparticles and hesperidin compound characterized using a FTIR 6100 spectrometer (Jasco, Japan) in the range of 4000 – 400 cm^{-1}.

2.5.3. Transmission electron microscopy (TEM)

The morphology and the particle size of ZnO NPs mediated by hesperidin were determined by TEM (JEOL-JEM-1011, Japan). Drops of the nanoparticles suspension were placed on carbon coated copper grid and the solvent was evaporated at the room temperature prior to recording the TEM image.

2.5.4. X-ray diffraction (XRD)

The ZnO NPs X-ray diffraction pattern recorded with PANLYTICAL X-ray diffractometer using Cu Kα radiation of wavelength 1d706; =0.1541 nm in the scan range 21d703; = 20−70˚.

2.6. Evaluation of the antiviral activity

The antiviral screening was performed using plaque inhibition assay at the Regional Center for Mycology and Biotechnology (RCMB, Al-Azhar University, Cairo, Egypt).

2.6.1. Mammalian cell line

Vero cells derived from African green monkey kidneys obtained from the American Type Culture Collection (ATCC, Manassas, VA, USA).

The Vero cells were propagated in Dulbecco's modified Eagle's medium (DMEM) supplemented with 10 % heat-inactivated fetal bovine serum (FBS), HEPES buffer, 1% L-glutamine and 50 µg/mL gentamycin. All cells were cultured at 37 °C in a humidified atmosphere with 5% CO_2 and were sub cultured two times for 7 days [14].

2.6.2. Cytotoxicity evaluation

Cytotoxicity assays were performed using Vero cells that implanted in 96-well plates at a cell concentration of 2×10^5 cells per ml in 100 µl of the growth medium. Fresh media containing different concentrations of hesperidin and ZnO NPs were added after 24 h of implantation. Serial two-fold dilutions of the tested samples (started from 3000 µg/mL to 2 µg/mL) were added to confluent cell monolayers dispensed into 96-well, flat-bottomed microtiter plates (Falcon, Jersey, NJ, USA) using a multichannel pipette. The microtiter plates were incubated at 37 °C in a humidified incubator with 5% CO_2 for a period of 2 days. Three wells were used for each concentration of the investigated samples. Control cells were incubated without test samples and with or without DMSO.

After the incubation period, the viable cell yield was determined by a MTT colorimetric assay [15]. The relation between surviving cells and the concentration of tested samples were plotted to obtain the survival curves of the Vero cell line after treatment with the specified compounds. The 50 % cytotoxic concentration (CC_{50}), the concentration required to cause toxic effects in 50 % of intact cells, was estimated from graphic plots of the dose response curve for each concentration using GraphPad Prism software (San Diego, CA. USA). The maximum nontoxic concentration [MNTC] of each hesperidin and ZnO NPs were determined and used for further biological studies.

2.6.3. Virus propagation

The cytopathogenic HAV HM175 strain (ATCC VR-1402) of HAV was propagated and assayed in confluent Vero cells [16]. Infectious viruses were enumerated by determining the 50 % tissue culture infectious dose with eight wells per dilution and 20 µL of inoculum per well using the Spearman-Karber method [17].

3. Results and discussion

Ten nutraceuticals phenolic compounds were selected according to their availability and spreading as a pharmaceutical dosage forms derived from natural nutritive food sources.

These nutraceuticals were diosmin, rutin, naringenin, quercetin 3-*O*-glucouronide, myricetin 3-O-xylosyl-(1→2)-rhamnoside, myricetin, epigallocatechin-3-*O*-gallate, corilagin and lyoniresinol. Hesperidin, diosmin and rutin are widely available in pharmaceutical stores under various trade names and can be derived from various natural nutritive foods reported to have antiviral properties for example, hesperidin from citrus peels has been reported to have antiviral activity [18]. On the basis of *in silico* screening hesperidin was also predicted to target the interaction site between SARS-CoV-2 Spike and ACE2 receptors, thus blocking the entry of the virus into the human lung cells. Therefore, hesperidin could be a promising prophylactic drug against COVID-19 [19].

In addition, naringenin from citrus peels were reported as antiviral agent against Zika virus [20], rutin [21] showed a significant results as antiviral [19]. Green tea's epigallocatechin-3-*O*-gallate has antiviral effects against a number of DNA and RNA viruses [22]. Corilagin prevents liver damage by inhibiting HCV replication and modulating oxidative stress [23]. Anti-HIV activity has been reported for myricetin and its glycosylated derivatives [24]. In addition, Several lignans have been reported to have antiviral properties [25].

Table 1
The binding mode, type of interaction and binding energy of phenolic compounds.

Compound	Binding mode	Type of interaction	Binding Energy (Kcal/mol)
Hesperidin with M^{pro}	THR 25, LEU 27, HIS 41, ASN 119, SER 123, LEU141, GLY 143, CYS 145.	Van der Waals	−8.84
	THR 24	Conv-HB	
	MET 49	Pi-alkyl	
	TYR 118	Pi-Pi Stacked	
Hesperidin with HAV 3C Proteinase	THR 26, ASN 142	C-HB	−6.91
	LYS146, LEU168, GLY194, GLY195, SER197	Van der Waals	
	PRO169	C-HB	
	ASN196	Amide-Pi Staked	
Myricetin-3-*O*-xylosyl-(1→2)-rhamnoside	HIS41, CYS44, THR45, MET49, TYR118, ASN142, GLY143	Van der Waals	−8.61
	THR 24, THR 25	Conv- HB	
	SER46	C-HB	
Diosmin	THR25,THR 26,THR 45, MET 49 ASN119, LEU141, ASN 142, GLY143, GLN189	Van der Waals	−8.59
	THR 24, SER 46	Conv- HB	
	THR 24	C-HB	
	TYR 118	Pi-Pi Stacked	
Epigallocatechin-3-*O*-gallate	THR26, LEU 27, HIS41, MET 49, ASN 142, GLY 143	Van der Waals	−7.91
	THR 24, THR 25	Conv- HB	
	THR 24	Amide-Pi Stacked	

Compound	Binding mode	Type of interaction	Binding Energy (Kcal/mol)
Rutin	THR 25, THR 26, LEU 27, HIS 41, MET 49,TYR 118,ASN 142, GLY 143, CYS 145, GLN 189	Van der Waals	−8.82
	THR 24, SER 46,	Conv- HB	
Quercetin 3-*O*-glucouronide	THR26, LEU 27, CYS 44, SER46,	Van der Waals	−8.01
	THR 24,	Pi-Donor HB	
	THR 25, THR 45, ASN 142, GLY 143	Con HB	
Coirlagin	LEU27, HIS41, THR 45,GLN 189	Van der Waals	−7.84
	MET 49	Pi-Sulfur	
	THR 25, SER46,GLY 143	Carbon HB	
	THR 24, THR 26, ASN 142, CYS 145	Conv-HB	
Myricetin	THR 24, THR 25, LEU 27, SER 46, GLY143, CYS 145	Van der Waals	−7.15
	THR26	Conv-HB	
Naringenin	LEU 4, THR 24, THR 25, THR 26,LEU 27, HIS 41, ASN 119, ASN 142, CYS 145	Van der Waals	−6.60
	GLY 143	Pi- Cation	
Lyoniresinol	THR 24, THR 45, SER 46, ASN 119, ASN142, GLY 143, CYS 145,	Van der Waals	−6.82
	THR 25, THR 26	Conv-HB	
	LEU 27, HIS 41, MET 49	Pi-alkyl	

3.1. Molecular docking

In the current research, an attempt was made to interpert and support the experimental findings regarding the inhibition mechanism of the main protease COVID-19. Ten polyphenolic compounds were docked using Swiss Dock Server, where receptor based approaches were applied to these polyphenols. The crystal structure of Covid-19 protease **6lu7**, which adopts a heart shape, with two dimers of identical subunits and two active sites. a broad-spectrum inhibitor should target the active site **His 41** and **Cys 148** of the progenitor bat coronavirus, as in PDB entry **4yoi**. This study eluciduated the binding mode of the phenolic compounds to the crystal structure **6lu7** by means of molecular docking (Fig. 2). The docking study confirmed that hesperidin can form electrostatic interactions with **THR 25, LEU 27, His 41** and **Gly143** residues while form pi-stacking interaction with **TYR 118** as listed in Table 1.

Most of the polyphenolic compounds showed inhibiton activity in the cleft region between domain II, III (residues 185–200) and In domain I as seen in Fig. 2 while in Table 1. the polyphenolic compounds listed according to their binding energies. The relationship of RMSD to the native binding mode (the full fitness (blue, left X-axis)) and energy (the simple fitness (red, right y-axis)) was been shown in Fig. **A,** (suppl.file). Docking mode for hesperidin was shown in (Figs.B for SARS-CoV-2 M^{pro} and Fig. C for HAV 3C Proteinase [26], 2HAL crystal structure), myricetin (Fig. D,1,2), diosmin(Fig. E 1,2), epigallocatechin-3-*O*-gallate (Figs F1,2), rutin (Figs G1,2), quercetin 3-*O*-glucouronide (Figs H 1,2), coirlagin (Figs I1,2), myricetin (Figs J1,2), naringenin (Figs L1,2) and lyoniresinol (Figs M1,2), in the supplementary file.

3.2. Isolation and identification of hesperidin

As hesperidin showed the highest docking score, herein, we isolated it from a food waste (orange peels) and its antiviral activity against HAV (one of the RNA viruses) was evaluated.

The butanol fraction from the aqueous extract of the orange peels was applied to Whatman filter paper sheets using BAW as an eluent, whereby, a major dark purple band of flavonoidal nature on the preparative paper chromatography was observed. Elution of the major dark purple band with methanol led to isolation of a pure compound that its identity was confirmed by ^{1}H, ^{13}C to be hesperidin [27] as follow: **^{1}H NMR** (400 MHz, DMSO-d_6 δ 5.50 (dd, J = 12.2, 3.4 Hz, 1H, H-2), 2.78 (dd, J =3.24 Hz & 17.16, 1H, H-3_{ax}), 3.26 (dd, J = 17.16, 8.22 Hz, 1H, H-3_{eq}), 6.14 (brs, 1H, H-6), 6.12 (brs, 1H, H-8), 4.97 (d, J =7.2 Hz, 1H, H-1″), 4.53 (s, 1H, H-1‴), 1.09 (d, J = 6.2, 3H, CH_3 of rhamnose). **^{13}C NMR** (101 MHz, DMSO-d_6) δ 78.89 (C-2), 42.74(C-3),197.48 (C-4), 163.50 (C-5), 96.85 (C-6), 165.60 (C-7), 96.00 (C-8), 162.96 (C-9), 103.79 (C-10), 131.35 (C-1′), 118.42 (C-2′), 146.92 (C-3′), 148.43 (C-4′), 112.50 (C-5′), 114.60 (C-6′), 56.15 (O-Me), 99.91(C-1″), 73.45 (C-2″), 76.73 (C-3″), 70.06 (C-4″), 75.98 (C-5″), 66.50 (C-6″), 101.06 (C-1‴), 70.73 (C-2‴), 71.17 (C-3‴), 72.53 (C-4‴), 68.78 (C-5‴), 18.29 (CH_3 of rhamnose; C-6‴).

3.3. ZnO nanoparticles formation

The addition of zinc acetate solution to hesperidin solution in water bath heated up to 80 °C followed by the addition of few drops of ammonia led to the precipitation of ZnO NPs [13].

3.3.1. UV analysis

The maximum absorption peak for ZnO NPs synthesized via hesperidin showed a peak at 335 nm (Fig. 3a) confirming the formation of ZnO NPs [28]. ZnO on a nano scale has shorter wavelengths compared with the standard ZnO absorption pattern, in agreement with reports that material oxides tend to have shorter wavelengths and that nanoscale materials tend to have shorter wavelengths [29].

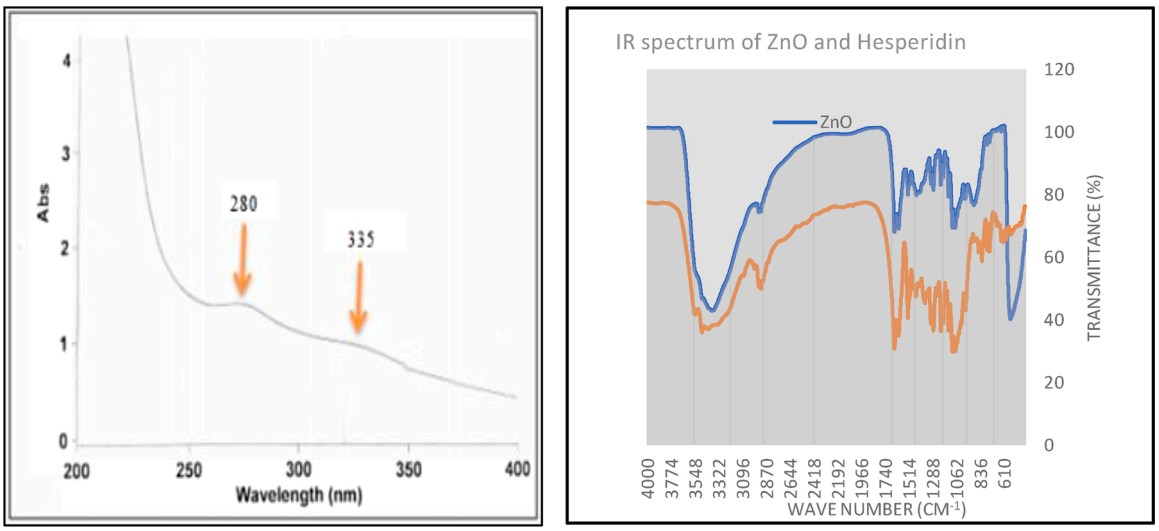

Fig. 3. a. UV spectrum of ZnO NPs b. IR Spectrum of hesperidin mediated zinc oxide nanoparticles.

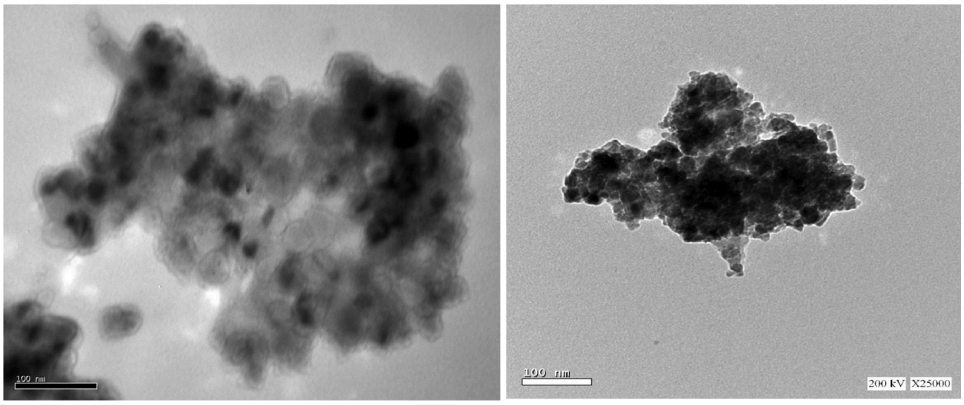

Fig. 4. TEM spectrum of ZnO NPs mediated by orange peels hesperidin (a. low resolution b. high resolution).

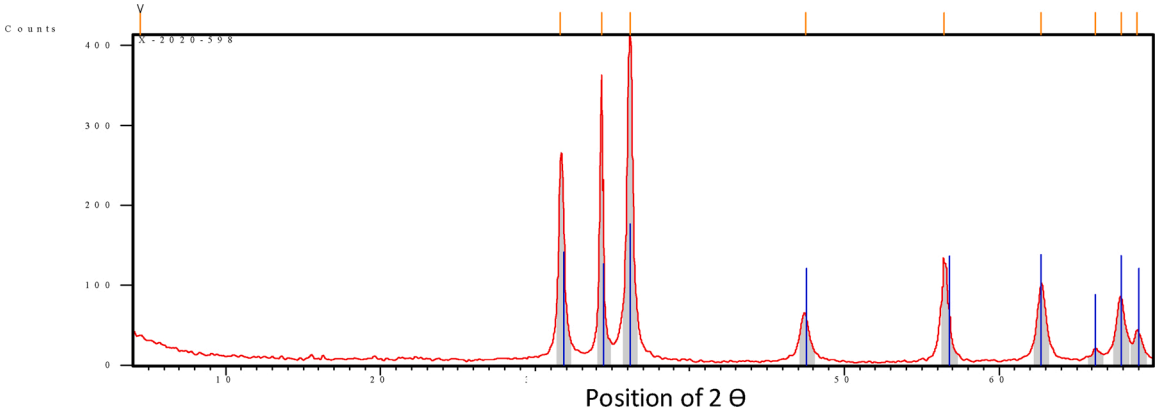

Fig. 5. XRD of ZnO NPs mediated by Hesperidin.

3.3.2. *FT-IR analysis of ZnO NPs and hesperidin*

FT-IR spectra (Fig. 3b) of the prepared ZnO NPs and hesperidin were collected in the spectral width range from 400 to 4000 cm^{-1}. Where showed peaks for O—H groups stretching of water around 3546.04, 3478.29 and 3421.80 cm^{-1} represent O—H groups of hesperidin and around 3382.99 cm^{-1} for ZnO NPs. Aromatic moieties were confirmed by carbon double bond stretching at 2918.50 cm^{-1}. Bending vibration of the alcoholic —CO—H confirmed by the presence of peak at 1096.12 cm^{-1}. The characteristic bands of the ZnO NPs stretching modes are assigned at 542.9 and 891.2 cm^{-1} [13,30].

3.3.3. *TEM analysis*

TEM analysis was performed on low resolution and high resolution transmission electron microscopes and showed the formation the hexagonal ZnO NPs with particle size ranging from 20 to 30 nm, Fig. 4.

3.3.4. XRD analysis

The occurrence of ZnO NPs and investigation of their structural features were confirmed by X-ray diffraction (XRD), Fig. 5. ZnO NPs mediated by the flavonoid hesperidin showed peaks with 2θ values identified at 31.618°, 34.334°, 36.161°, 47.504°, 56.440°, 62.727°, 66.245°, 67.864°, and 68.925° corresponding to (100), (002), (101), (102), (110), (103), (200), (112) and (201). These peaks were matched with those of data card (00−003-0888).

The crystal size of ZnO NPs was calculated to be 27.73 nm. This data is very similar to TEM measurements. To calculate the crystal size we apply Scherrer's equation

$$\text{Crystal Size} = (0.9 \times \lambda)/(d\cos\theta)$$

$\Theta = 2\theta/2$, d = the full width at half maximum intensity of the peak (in Rad), λ =0.154060 nm

3.4. Antiviral activity

3.4.1. Evaluation of cytotoxicity against Vero cells

The two samples of hesperidin and ZnO NPs showed 50 % cell cytotoxic concentration (CC_{50}) = 620.8 ± 34.6 and 243.7 ± 12.7 μg/mL, respectively. As shown if Figs. K. &L., suppl. file and the values were listed in tables C & D. respectively. Then, these compounds were tested for antiviral effects against HAV at the maximum non-toxic concentration (MNTC) using plaque assay method illustrated in Fig. M. (supplementary file).

3.4.2. Anti-HAV activity

Flavonoids have been reported to have antiviral activities both *in vivo* and *in vitro* [31]. It was reported that the mechanism of action of some flavonoids against HIV (also an RNA virus) is due to the inhibition of phosphorylation of proteins mediated by cytokines. It should also be noted that the phosphorylation signaling mediated by cytokines is increased in COVID-19 infection, leading to the phosphorylation of numerous cytoskeletal proteins. Therefore, flavonoids, which include hesperidin, can inhibit protein phosphorylation, which in turn leads to potent antiviral activity and infection prevention of other cells [32]. ZnO NPs have also been reported to have antiviral activity [32,33].

Zn-containing compounds reported to affect diverse stages of viral replication cycles such as virus inactivation, inhibition of viral uncoating, viral genome transcription, viral protein translation and polyprotein processing. It should be noted also that the activity dependent on the type of the virus and the concentration of zinc containing compounds [34].

In our study, the confluent monolayers of vero cells were infected with fixed dilutions of HAV virus. After incubation, inoculum was removed and replaced with serum-free MEM containing 1.5 % carboxymethyl cellulose. The cells were then incubated allowing the virus to form the plaques.The cells were fixed for 2 h at 25 °C with formaldehyde that added directly to the medium till concentration of 5%. Fixed cells were extensively washed with water before being stained with a solution containing 1% crystal violet and 10 % ethanol for 30 min. After rinsing with water, the number of plaques was counted, and virus titers (counts) were calculated. The antiviral effects of the two tested samples, hesperidin and ZnO NPs against HAV at maximum noncytotoxic concentration (MNCC) are shown in the Table B (supplementary file). The zinc oxide nanoparticles showed higher activity than hesperidin at relatively low concentration due to the high surface area and small particle size, which increased the activity of zinc oxide nanoparticles. From the Table B, Fig. T, (supplementary file). Both hesperidin and ZnO NPs showed antiviral activity against Hepatitis A virus (HAV) with percentages of 44.75 and 58.83 % at maximum noncytotoxic concentration and EC_{50}s equal to 72.4 and 176.3 μg/mL, respectively as shown in the Tables A and B (supplementary file).

4. Conclusions

The current pandemic disease COVID-19 is responsible for a lot of morbidity and mortality worldwide. Nutraceuticals and phytopharmaceuticals phenolic compounds under our study exhibit good docking scores and it could be an ideal targets for treatment of SARS-CoV-2. Hesperidin which is isolated from food waste orange peels is exhibited the highest docking score (-8.84 Kcal/mol) against SARS-CoV-2 main protease among the other tested compounds. Hesperidin is capable of reduction of zinc ions to prepare ZnO NPs with hexagonal shape and particles size about 25 nm. Hesperidin mediated ZnO NPs exhibit antiviral activity than hesperidin itself with percentages of 44.75 and 58.83 % at maximum noncytotoxic concentration. More studies should be done for hesperidin, other nutraceutical, phytopharmaceutical compounds and their ZnO NPs for finding a safe, cheap and potential treatments for SARS-CoV-2 pandemic disease.

Authors contributions

Gouda H. Attia, Yasmin S. Moemen, Mahmoud Youns, Ammar M. Ibrahim, Randa Abdou, Mohamed A. El Raey

Gouda H. Attia and Mohamed A. El Raey design the manuscript.

Gouda H. Attia, Ammar M. Ibrahim and Mohamed A. El Raey conducted the chromatographic separation and performed the structure elucidation of the pure isolated Hesperidin

Gouda H. Attia, Randa Abdou and Mohamed A. El Raey performed green synthesis of ZnO NPs and describe its features.

Yasmin S. Moemen performed all the molecular docking study and Mohamed A. El-Raey suggest the protein.

Mahmoud Youns and Randa Abdou performed the antiviral and cytotoxicity assays and their data analysis.

All authors were responsible for drafting and writing the final version of the manuscript and approved the final manuscript.

Funding

No funding was received for this work.

Research ethics

We further confirm that any aspect of the work covered in this manuscript that has involved human patients has been conducted with the ethical approval of all relevant bodies and that such approvals are acknowledged within the manuscript.

IRB approval was obtained (required for studies and series of 3 or more cases)

Written consent to publish potentially identifying information, such as details or the case and photographs, was obtained from the patient(s) or their legal guardian(s).

Declaration of Competing Interest

The authors report no declarations of interest.

Acknowledgments

We are grateful to the Deanship of Scientific Research, Najran University, KSA, for providing the funding to perform this project (NU/MID/18/024).

Appendix A. Supplementary data

Supplementary material related to this article can be found, in the online version, at doi:https://doi.org/10.1016/j.colsurfb.2021.111724.

References

[1] World Health Organization, WHO Coronavirus Disease (COVID-19), 2020 (Accessed October 22, 2020), https://www.worldometers.info/coronavirus/#countries.

[2] J. Hunter, S. Arentz, J. Goldenberg, G. Yang, J. Beardsley, D. Mertz, S. Leeder, Rapid review protocol: zinc for the prevention or treatment of COVID-19 and other coronavirus-related respiratory tract infections, Integr. Med. Res. 9 (2020), 100457.

[3] G.J. Kotwal, Antiviral nutraceuticals from pomegranate (Punica granatum) juice, in: Handb. Nutraceuticals, Vol. I, CRC Press, 2009, pp. 338–346.

[4] L.-T. Lin, W.-C. Hsu, C.-C. Lin, Antiviral natural products and herbal medicines, J. Tradit. Complement. Med. 4 (2014) 24–35.

[5] A. Kumar, Y. Kubota, M. Chernov, H. Kasuya, Potential role of zinc supplementation in prophylaxis and treatment of COVID-19, Med. Hypotheses (2020), 109848.

[6] J. Jiang, J. Pi, J. Cai, The advancing of zinc oxide nanoparticles for biomedical applications, Bioinorg. Chem. Appl. (2018), https://doi.org/10.1155/2018/1062562.

[7] A.J.W. Te Velthuis, S.H.E. van den Worm, A.C. Sims, R.S. Baric, E.J. Snijder, M. J. van Hemert, Zn2+ inhibits coronavirus and arterivirus RNA polymerase activity in vitro and zinc ionophores block the replication of these viruses in cell culture, PLoS Pathog. 6 (2010), e1001176.

[8] Z. Jin, X. Du, Y. Xu, Y. Deng, M. Liu, Y. Zhao, B. Zhang, X. Li, L. Zhang, C. Peng, Structure of M pro from SARS-CoV-2 and discovery of its inhibitors, Nature (2020) 1–5.

[9] A. Grosdidier, V. Zoete, O. Michielin, SwissDock, a protein-small molecule docking web service based on EADock DSS, Nucleic Acids Res. (2011), https://doi.org/10.1093/nar/gkr366.

[10] A. Kucukelbir, F.J. Sigworth, H.D. Tagare, Quantifying the local resolution of cryo-EM density maps, Nat. Methods 11 (2014) 63–65.

[11] H.H. Barakat, M. El-Raey, S.A. Nada, I. Zeid, M. Nawwar, Constitutive phenolics and hepatoprotective activity of Eugenia supra-axillaris leaves, EJ Chem. 54 (2011) 313–323.

[12] S.M. Osman, W.A. El Kashak, M. Wink, M.A. El Raey, New isorhamnetin derivatives from Salsola imbricata Forssk. Leaves with distinct anti-inflammatory activity, Pharmacogn. Mag. 12 (2016) S47.

[13] G.H. Attia, H.S. Alyami, M.A.A. Orabi, A.H. Gaara, M.A. El Raey, Antimicrobial activity of silver and zinc nanoparticles mediated by eggplant green Calyx, Int. J. Pharmacol. 16 (2020) 236–243.

[14] P. Vijayan, C. Raghu, G. Ashok, S.A. Dhanaraj, B. Suresh, Antiviral activity of medicinal plants of Nilgiris, Indian J. Med. Res. 120 (2004) 24–29.

[15] T. Mosmann, Rapid colorimetric assay for cellular growth and survival: application to proliferation and cytotoxicity assays, J. Immunol. Methods 65 (1983) 55–63.

[16] W. Randazzo, J. Piqueras, J. Rodríguez-Díaz, R. Aznar, G. Sánchez, Improving efficiency of viability-qPCR for selective detection of infectious HAV in food and water samples, J. Appl. Microbiol. 124 (2018) 958–964.

[17] R.M. Pintó, J.M. Diez, A. Bosch, Use of the colonic carcinoma cell line CaCo-2 for in vivo amplification and detection of enteric viruses, J. Med. Virol. 44 (1994) 310–315.

[18] Z. Ding, G. Sun, Z. Zhu, Short communication Hesperidin attenuates influenza A virus (H1N1) induced lung injury in rats through its anti-inflammatory effect, Antivir. Ther. 23 (2018) 611–615.

[19] C. Wu, Y. Liu, Y. Yang, P. Zhang, W. Zhong, Y. Wang, Q. Wang, Y. Xu, M. Li, X. Li, Analysis of therapeutic targets for SARS-CoV-2 and discovery of potential drugs by computational methods, Acta Pharm. Sin. B (2020).

[20] A.H.D. Cataneo, D. Kuczera, A.C. Koishi, C. Zanluca, G.F. Silveira, T.B. de Arruda, A.A. Suzukawa, L.O. Bortot, M. Dias-Baruffi, W.A. Verri, The citrus flavonoid naringenin impairs the in vitro infection of human cells by Zika virus, Sci. Rep. 9 (2019) 1–15.

[21] Y.-J. Lin, Y.-C. Chang, N.-W. Hsiao, J.-L. Hsieh, C.-Y. Wang, S.-H. Kung, F.-J. Tsai, Y.-C. Lan, C.-W. Lin, Fisetin and rutin as 3C protease inhibitors of enterovirus A71, J. Virol. Methods 182 (2012) 93–98.

[22] K. Kaihatsu, M. Yamabe, Y. Ebara, Antiviral mechanism of action of epigallocatechin-3-O-gallate and its fatty acid esters, Molecules 23 (2018) 2475.

[23] B.U. Reddy, R. Mullick, A. Kumar, G. Sharma, P. Bag, C.L. Roy, G. Sudha, H. Tandon, P. Dave, A. Shukla, A natural small molecule inhibitor corilagin blocks HCV replication and modulates oxidative stress to reduce liver damage, Antiviral Res. 150 (2018) 47–59.

[24] J.T. Ortega, A.I. Suárez, M.L. Serrano, J. Baptista, F.H. Pujol, H.R. Rangel, The role of the glycosyl moiety of myricetin derivatives in anti-HIV-1 activity in vitro, AIDS Res. Ther. 14 (2017) 1–6.

[25] R.B. Teponno, S. Kusari, M. Spiteller, Recent advances in research on lignans and neolignans, Nat. Prod. Rep. 33 (2016) 1044–1092.

[26] J. Yin, M.M. Cherney, E.M. Bergmann, J. Zhang, C. Huitema, H. Pettersson, L. D. Eltis, J.C. Vederas, M.N.G. James, An episulfide cation (thiiranium ring) trapped in the active site of HAV 3C proteinase inactivated by peptide-based ketone inhibitors, J. Mol. Biol. 361 (2006) 673–686.

[27] V.M. Chari, M. Jordan, H. Wagner, P.W. Thies, A 13C-NMR study of the structure of an acyl-linarin from Valeriana wallichii, Phytochemistry 16 (1977) 1110–1112.

[28] N. Srinivasan, C. Rangasami, J.C. Kannan, Synthesis structure and optical properties of zinc oxide nanoparticles, Int J Appl Eng Res. 10 (2015) 343–345.

[29] S. Fakhari, M. Jamzad, H. Kabiri Fard, Green synthesis of zinc oxide nanoparticles: a comparison, Green Chem. Lett. Rev. 12 (2019) 19–24.

[30] N. Bala, S. Saha, M. Chakraborty, M. Maiti, S. Das, R. Basu, P. Nandy, Green synthesis of zinc oxide nanoparticles using Hibiscus subdariffa leaf extract: effect of temperature on synthesis, anti-bacterial activity and anti-diabetic activity, RSC Adv. 5 (2015) 4993–5003.

[31] H. Zakaryan, E. Arabyan, A. Oo, K. Zandi, Flavonoids: promising natural compounds against viral infections, Arch. Virol. 162 (2017) 2539–2551.

[32] M. Bouhaddou, D. Memon, B. Meyer, K.M. White, V.V. Rezelj, M.C. Marrero, B. J. Polacco, J.E. Melnyk, S. Ulferts, R.M. Kaake, The global phosphorylation landscape of SARS-CoV-2 infection, Cell 182 (2020) 685–712.

[33] H. Ghaffari, A. Tavakoli, A. Moradi, A. Tabarraei, F. Bokharaei-Salim, M. Zahmatkeshan, M. Farahmand, D. Javanmard, S.J. Kiani, M. Esghaei, Inhibition of H1N1 influenza virus infection by zinc oxide nanoparticles: another emerging application of nanomedicine, J. Biomed. Sci. 26 (2019) 1–10.

[34] S.A. Read, S. Obeid, C. Ahlenstiel, G. Ahlenstiel, The role of zinc in antiviral immunity, Adv. Nutr. 10 (2019) 696–710.